



Review

Characterization of Structural Bone Properties through Portable Single-Sided NMR Devices: State of the Art and Future Perspectives

Marco Barbieri ^{1,2,*} , Paola Fantazzini ² , Claudia Testa ^{2,3} , Villiam Bortolotti ⁴ , Fabio Baruffaldi ⁵ , Feliks Kogan ¹ and Leonardo Brizi ^{2,*}

- ¹ Department of Radiology, Stanford University, Stanford, CA 94395, USA; fkogan@stanford.edu
² Department of Physics and Astronomy “Augusto Righi”, University of Bologna, 40127 Bologna, Italy; paola.fantazzini@unibo.it (P.F.); claudia.testa@unibo.it (C.T.)
³ IRCCS Istituto delle Scienze Neurologiche Bologna, Functional and Molecular Neuroimaging Unit, 40139 Bologna, Italy
⁴ Department of Civil, Chemical, Environmental, and Materials Engineering, University of Bologna, 40134 Bologna, Italy; villiam.bortolotti@unibo.it
⁵ Medical Technology Laboratory, IRCCS Istituto Ortopedico Rizzoli, 40136 Bologna, Italy; fabio.baruffaldi@ior.it
* Correspondence: mb7@stanford.edu (M.B.); leonardo.brizi2@unibo.it (L.B.)

Abstract: Nuclear Magnetic Resonance (NMR) is a well-suited methodology to study bone composition and structural properties. This is because the NMR parameters, such as the T_2 relaxation time, are sensitive to the chemical and physical environment of the ^1H nuclei. Although magnetic resonance imaging (MRI) allows bone structure assessment in vivo, its cost limits the suitability of conventional MRI for routine bone screening. With difficulty accessing clinically suitable exams, the diagnosis of bone diseases, such as osteoporosis, and the associated fracture risk estimation is based on the assessment of bone mineral density (BMD), obtained by the dual-energy X-ray absorptiometry (DXA). However, integrating the information about the structure of the bone with the bone mineral density has been shown to improve fracture risk estimation related to osteoporosis. Portable NMR, based on low-field single-sided NMR devices, is a promising and appealing approach to assess NMR properties of biological tissues with the aim of medical applications. Since these scanners detect the signal from a sensitive volume external to the magnet, they can be used to perform NMR measurement without the need to fit a sample inside a bore of a magnet, allowing, in principle, in vivo application. Techniques based on NMR single-sided devices have the potential to provide a high impact on the clinical routine because of low purchasing and running costs and low maintenance of such scanners. In this review, the development of new methodologies to investigate structural properties of trabecular bone exploiting single-sided NMR devices is reviewed, and current limitations and future perspectives are discussed.

Keywords: bone; single-sided NMR; NMR relaxometry; osteoporosis; structural parameters



Citation: Barbieri, M.; Fantazzini, P.; Testa, C.; Bortolotti, V.; Baruffaldi, F.; Kogan, F.; Brizi, L. Characterization of Structural Bone Properties through Portable Single-Sided NMR Devices: State of the Art and Future Perspectives. *Int. J. Mol. Sci.* **2021**, *22*, 7318. <https://doi.org/10.3390/ijms22147318>

Academic Editor: Alberto Falchetti

Received: 7 June 2021

Accepted: 2 July 2021

Published: 7 July 2021

Publisher's Note: MDPI stays neutral with regard to jurisdictional claims in published maps and institutional affiliations.



Copyright: © 2021 by the authors. Licensee MDPI, Basel, Switzerland. This article is an open access article distributed under the terms and conditions of the Creative Commons Attribution (CC BY) license (<https://creativecommons.org/licenses/by/4.0/>).

1. Introduction

Osteoporosis is a disease associated with increased bone fragility and susceptibility to fractures, which poses a high economic burden on health systems and has a severe impact on the quality of human health [1–3]. People experiencing an osteoporotic fracture are exposed to various adverse outcomes in terms of morbidity, subsequent fractures, and mortality after hospital discharge [4]. Methodologies aiming to improve early and accurate assessment of the fracture risk related to osteoporosis are necessary to effectively treat osteoporotic patients to prevent the worsening of bone health before a fragility fracture occurs. Wide campaigns of screening the population at risk of osteoporosis are desirable,

which motivates the development of techniques that are low-cost and easily accessible to allow routine application.

Dual-energy X-ray absorptiometry (DXA) is currently the most commonly utilized clinical tool for the diagnosis of osteoporosis [5]. It employs ionizing radiation and provides a measure of the areal bone mineral density (BMD), but it does not provide information about the architecture of the bone [3,6]. Other than BMD, bone strength depends on the size, shape, architecture, and composition of the tissue [5]. For example, the resilience of the trabecular bone depends not only on BMD but also on the architecture of the trabecular structure. Furthermore, epidemiological studies showed that BMD is a poor predictor of fracture risk, the low values of BMD being able to explain about 50% of the incident fracture cases [7]. Models for risk fracture evaluation that integrate BMD with anthropometric factors, lifestyle factors, and comorbidities have been proposed and shown to increase fracture risk prediction accuracy [8,9]. Despite the evidence that bone strength, and by consequence the fracture risk, also depends on bone architecture and composition, there are no well-studied models that incorporate information about bone architecture or composition in fracture risk assessment. This is largely due to the absence of an exam able to provide such information that is suitable for routine clinical practice.

Although high-resolution quantitative Computed Tomography (HRqCT) can provide volumetric 3D measurements of cortical and trabecular bone *in vivo*, it requires a higher X-ray dose than DXA, is more expensive, and is primarily limited to peripheral skeleton bones. Therefore, the use of these scans in a clinical setting is infrequent [5]. Quantitative ultrasounds (qUS) have also been proposed as prescreening methodology for study bone mineralization and some structural properties [10] and have the advantage of being low-cost and do not use ionizing radiation. Although qUS-based techniques for bone assessment have been around since the early 1990s [10], measurements are still affected by low repeatability and reproducibility [11,12].

Nuclear Magnetic Resonance (NMR) is a well-suited technology to study bone structural properties and its composition. It does not use ionizing radiation, and laboratory studies have shown the ability of NMR to assess properties of bone with different techniques, ranging from relaxometry to diffusometry and Magic Angle Spinning [13–22]. Although clinical magnetic resonance imaging (MRI) allows bone structure assessment *in vivo* [23–25], its cost limits the suitability of conventional MRI for routine bone screening. The use of more compact and lower magnetic field scanners has been proposed to lower the cost of MRI analyses for imaging trabecular bone structure on peripheral body regions [26,27]. Furthermore, bone is a complex tissue, and assessment of bone properties with quantitative MRI in acquisition times suitable for clinical application is challenged regarding the need of spatially encoding the NMR signal.

Portable NMR, based on low-field single-sided NMR devices, is a promising and appealing approach to assess NMR properties of biological tissues, particularly for relaxometry and diffusometry, with the aim of medical applications. The main feature that differentiates a single-sided apparatus from other NMR scanners is the detection of the signal from a sensitive volume external to the magnet. Therefore, such devices can be used to perform NMR measurement without the need to fit a sample inside a bore of a magnet, allowing, in principle, *in vivo* application not limited to peripheral body sites. Moreover, the intrinsic magnetic field gradients can be used for spatial encoding. Portable NMR also has the added advantages of low purchasing, running, and maintenance costs, largely due to the absence of superconducting magnets (permanent magnets are employed instead). Portable NMR devices [28–34] have been applied in various fields such as agriculture [35], cultural heritage [36–38], porous media [39], and biomedicine including testing of silicone breast implants [40] and *ex vivo* studies of various biological tissues: tendon [41], articular cartilage [42,43], skin [44], breast [45], and bone tissue [46–50]. *In vivo* studies on humans have also been conducted on skin [51] and tendons [52].

In this review, the development of new methodologies to investigate trabecular bone properties in laboratory exploiting single-sided NMR devices is reviewed, and current

limitations and future perspectives are discussed. In Section 2, a brief background on NMR relaxometry of the bone tissue is provided. A few details about single-sided NMR devices are given in Section 3. Works investigating the characterization of trabecular bone structure using single-sided NMR are reviewed in Section 4. In Section 5, current limitations and future perspectives are discussed with a specific attention to the long-term aim, i.e., the extension of such techniques to an in vivo application.

2. NMR Relaxometry Properties of Bone Tissue

2.1. Bone Tissue and Osteoporosis: A Brief Background

Bone is a complex composite including type-I collagen, calcium phosphate mineral deposits, lipids, and water confined in a network of nano-, micro-, and macrostructural compartments. Bone can be classified in cortical bone (CB) and trabecular bone (TB), characterized by different structures. The components of CB are arranged in a porous space made of the Haversian canals and the lacunar-canalicular system, which occur in repeating cylindrical units called osteons. TB, predominant in the axial skeleton and near the joints of the long bones, consists of a network of interconnected trabeculae, typically 100–150 μm thick, where the lacunar-canalicular porosity and the collagen–apatite porosity is found, as for the cortical bone. In TB, there is further porosity contributed by the inter-trabecular space containing marrow, fat, and blood vessels, but not the Haversian canals.

The bone tissue experiences different loads in intensity and directions over life-time, which causes an adaptive response of the bone tissue, such as altering structural density and orientation (i.e., creating anisotropy) [53]. This adaptive response is possible because of bone remodeling, a process where bone tissue is removed by osteoclastic resorption and new bone is formed by osteoblasts. In the adult skeleton, the bone tissue is remodeled in a process that has a dynamic equilibrium between bone formation and bone resorption. With aging and in the context of osteoporosis, this equilibrium is broken, and the balance of bone resorption and formation becomes negative. Thus, the bone loss in aged and osteoporotic bone is a consequence of imbalanced and excessive bone remodeling [54], which increases fracture risk.

Since bone remodeling occurs on the surfaces of internal bone structures, osteoporotic bone loss is a function of the surface available for bone remodeling [55]. In individuals, less than 65 years of age, the trabeculae of the trabecular bone furnish the largest surface available for bone remodeling. In this population, trabecular bone provides only about 20% of the skeletal bone mass, but it is responsible for most of the turnover [53]. Thus, the bone loss in early osteoporosis is mainly due to trabecular bone [53]. With the advance of the disease, the porosity of the cortical bone increases as well, and, therefore, its endocortical surface increases. As a consequence, the largest loss of absolute bone mass due to osteoporosis in an advanced state occurs in cortical bone by intracortical remodeling [53]. These considerations allow one to appreciate the importance of assessing bone structural properties, and the importance of having techniques able to conveniently gain that information to allow early detection of osteoporotic behavior of the bone tissue. Some of the most common parameters for structure characterization of trabecular bone are:

- BONE VOLUME/TOTAL VOLUME, BV/TV (%): % of total volume of the trabeculae with respect to the total volume of the analyzed tissue;
- BONE SURFACE/TOTAL VOLUME, BS/TV (mm^{-1}): total external surface of the trabeculae with respect to the total volume of the analyzed tissue;
- TRABECULAR THICKNESS, Tb.Th (mm): the mean trabecular thickness found in the trabeculae of the analyzed tissue.

2.2. NMR Relaxation in Porous Media and Bone Tissue

In this section, the NMR signal of ^1H nuclei, usually called proton NMR, is considered. NMR relaxation parameters, such as T_1 and T_2 relaxation times, both depend on the chemical and physical environment of the ^1H nuclei and can be used to characterize these environments. The information provided by NMR relaxometry has constituted a powerful

non-invasive and non-destructive tool for studying the structural properties of porous media [14,56,57].

In biological tissues, ^1H nuclei can be present in different chemical environments (water or fat, for example), and some tissues, from an NMR perspective, can be modeled as porous media in which fluids are confined in complex porous structures. Thus, a multi-exponential relaxation process is often encountered. The acquired multi-exponential decay data can be analyzed by quasi-continuous T_1 and T_2 distributions, able to give unique information about the tissue under study. In the context of bones, the ^1H nuclei are found in different micro-environments that are too small to be spatially resolved with MRI, but their NMR signal contributions can be resolved in the time domain using the multi-exponential NMR relaxation approach.

NMR relaxometry investigations on cortical and trabecular bones have been extensively studied in the literature, and many studies have shown that T_2 relaxation times span a range that goes from tens of μs to hundreds of ms [14,15,25,49,58,59]. Hence, the different T_2 components can be mapped to the corresponding ^1H nuclei micro-environments.

Figure 1 summarizes the T_2 relaxation properties of human cortical bones found by Horch et al. [58,59] using quasi-continuous T_2 distributions, obtained by an inversion process of the Carr–Purcell–Meiboom–Gill (CPMG) measured data [60,61]. The T_2 distributions (Figure 1b) present two distinct sub-millisecond relaxation components, and a broad tail spanning the millisecond-second T_2 domain. The first sub-millisecond component ($T_2 \sim 60 \mu\text{s}$) has been attributed to the collagen methylene protons, while the second sub-millisecond component ($T_2 \sim 400 \mu\text{s}$) contains signal contributions from collagen-bound water and water within the lacunar-canalicular system (order $0.1 \mu\text{m}$ [62]). The long-lived tail spanning the millisecond-second domain contains signal contributions from water within the Haversian canals and lipids present within the cement lines (regions of collagen-poor bone matrix found at the outer border of osteons). It is important to note that the signal contributions due to water within Haversian canals and the lacunar-canalicular system is generally referred to as pore water. However, the spatial scale of pores within cortical bone varies considerably and thus the T_2 relaxation times vary accordingly to the size of the pore structure.

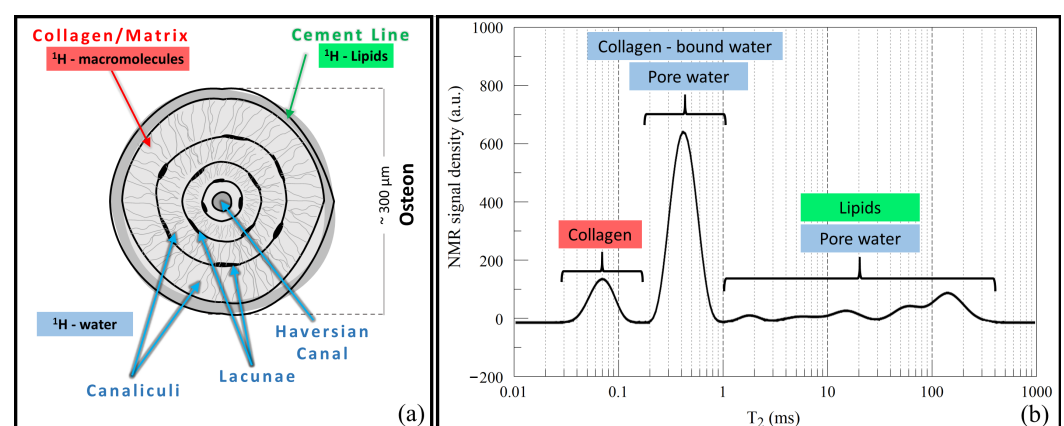


Figure 1. (a) Schematic representation of cortical bone indicating its constituents and compounds from which the ^1H NMR signal arises; (b) T_2 distribution of human cortical bone (plot from data presented in reference [58]).

Fantazzini et al. [14] conducted NMR relaxometry studies on animal trabecular bones finding that trabecular bone T_2 distributions present a distinct sub-millisecond relaxation component and a broad component spanning the millisecond-second domain that accounts for most of the signal. The first sub-millisecond component ($T_2 \sim 400 \mu\text{s}$) was attributed to signals coming from protons within the trabeculae (intra-trabecular signal), which includes collagen-bound water and pore water. The second component was attributed to fluids within the inter-trabecular spaces. Figure 2 presents a schematic representation of

trabecular bone along with a T_2 distribution obtained from a trabecular bone sample cored from a pig shoulder [50] to highlight the connection between the T_2 components and the trabecular bone constituents.

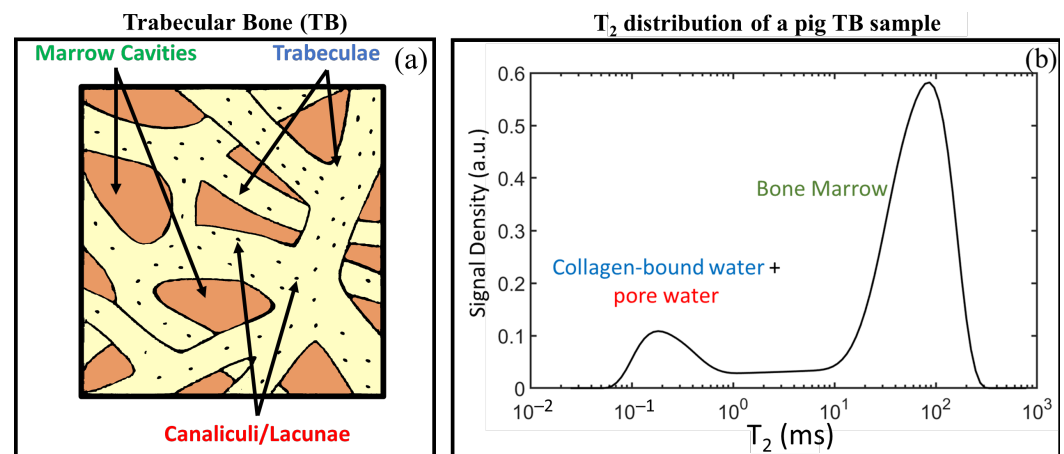


Figure 2. (a) Schematic representation of trabecular bone indicating its constituents; (b) T_2 distribution of a trabecular bone sample cored from a pig shoulder (plot from data used in reference [50]).

It is important to notice that MRI has been incorporating the concepts of NMR relaxometry in quantitative MRI (qMRI) methodologies such as T_1 and T_2 mapping. However, these methodologies are challenged by technical limitations that arise from the constraints imposed by the need to spatially encode the NMR signal. For these reasons, the majority of qMRI protocols that can be run in clinically acceptable times apply mono-exponential models to processes that often are multi-exponential.

3. Single-Sided NMR Devices

Single-sided NMR devices detect the signal from a sensitive volume positioned above the surface of the magnet and the radiofrequency (RF) coil, which implies that there are no strict requirements about the size of the sample to be investigated. They use permanent magnets to generate the polarizing field B_0 , usually on the order of hundreds of mT, with a significantly small size compared to high-field NMR and whole-body MRI scanners. Altogether, these characteristics make single-sided NMR scanners portable, low maintenance, low purchasing costs, and suitable for in situ measurements.

Different magnet geometries have been explored for single-sided NMR [28–34]. The main difference among these scanners is the design and disposition of the permanent magnets, which determines the polarizing magnetic field and consequently the position and shape of the sensitive volume, the volume where the ^1H nuclei will be excited by a suitable RF pulse. Two main classes can be differentiated, taking into account the distribution of the static magnetic field. In the first class [28,30–32], one or more magnets are used to generate a grossly inhomogeneous B_0 field, and an RF coil is designed such that the excitation field B_1 and the static field B_0 are orthogonal within a specific region above the surface of the magnet. The B_0 gradient and the excitation bandwidth define the sensitive volume. A sub-class of such devices generates a uniform constant B_0 gradient within the sensitive volume, allowing for diffusivity measurements [28,32,33]. The second class of instruments [29,31,34] generates a *sweet spot* at which B_0 is locally homogeneous. Figure 3 presents a schematic representation of two single-sided NMR devices belonging to the two classes described above. Until recently, the maximum penetration depth achieved by portable single-sided NMR devices ranged from a few mm to 2 cm. Thomas et al. [34] presented a novel single-sided NMR device with a maximum penetration depth of 50 mm.

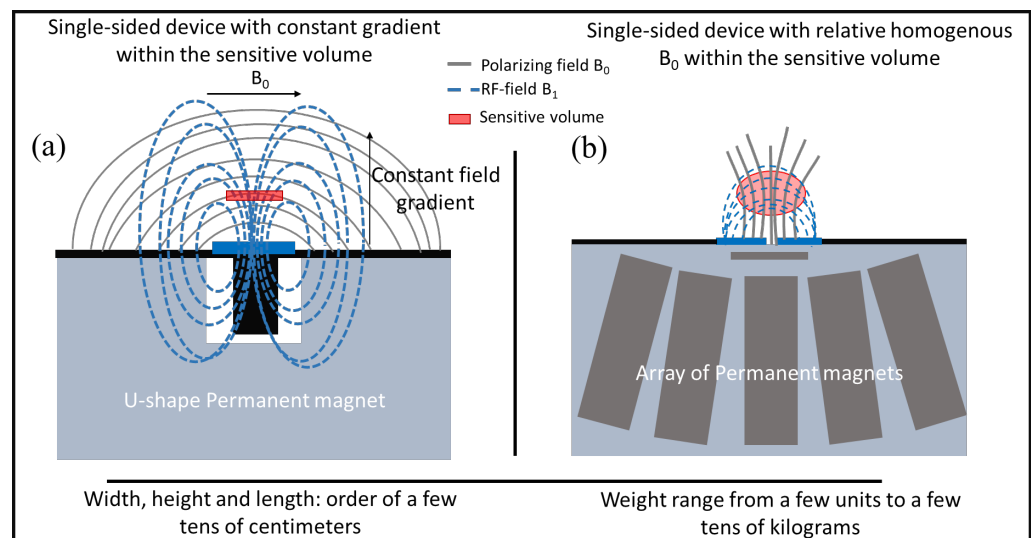


Figure 3. (a) Sketch of the design of a single-sided NMR device with a constant field gradient within the sensitive volume; (b) sketch of the design of a single-sided NMR device with a relative homogeneous B_0 within the sensitive volume.

4. Evaluating Trabecular Bone Structural Properties of Animal Samples with Single-Sided NMR

A procedure to assess the bone volume fraction of trabecular bone using single-sided NMR devices was first proposed in [47] in the laboratory using ex vivo animal samples. The procedure, whose pipeline is summarized in Figure 4, is based on computing the ratio between the CPMG signals obtained from a trabecular bone sample and the CPMG signal obtained from a reference bulk marrow sample. As long as the volumes of the samples intercepted by the sensitive volume of the single-sided NMR scanner are the same, the ratio of the two signals (where the signal is the total area under the T_2 distribution computed out of the CPMG decay) is proportional to the ratio between the volume of the bone marrow within the inter-trabecular spaces and the total volume of the sample. The bone volume fraction can then be evaluated according to Equation (1), where S_{TB} is the NMR signal from the marrow inside the trabecular bone sample, and S_{BM} is the NMR signal from a reference bulk marrow sample:

$$\frac{BV}{TV} = \left(1 - \frac{S_{TB}}{S_{BM}}\right) \times 100(\%) \quad (1)$$

The methodology was validated on a set of phantoms of which ground truth BV/TV could be accurately computed by their geometry and on a set of six trabecular bone samples where the micro-CT was used to estimate the reference BV/TV. The validation experiments presented in [47], reported in Figure 5, showed a high correlation between phantoms and trabecular bone samples.

A limitation of the procedure presented in [47] is the need to use a reference sample to compute the BV/TV ratio. If the volume of the reference sample differs from the volume of the trabecular bone intercepted by the sensitive volume of the single-sided NMR scanner, the evaluation of BV/TV is no longer accurate. Moreover, the need for an external reference could be a drawback in a possible future in vivo application. The procedure was then further developed in [50], reducing at least in part the need for a reference sample and extending the study to the estimation of the structural parameter BS/TV (% of the total external surface of the trabeculae with respect to the total volume of the analyzed tissue). These goals were achieved by optimizing the experimental set-up to maximize the Signal-to-Noise ratio, giving a physical interpretation to the T_2 quasi-continuous distributions, and by applying simple theoretical models to obtain NMR estimates of BV/TV and BS/TV. The NMR estimates obtained in laboratory using animal samples were validated by the

comparison with the values of these parameters measured by micro-CT analyses. Figure 6 summarizes the pipeline used to implement the methodology presented in [50] along with the theoretical models used to estimate BV/TV, BS/TV, and the intra-trabecular porosity, ϕ_{tb} . The latter parameter was first introduced in [15] and is defined as the volume within the trabeculae occupied by the fluids divided by the total volume of the trabeculae. The reader is invited to read reference [50] for a detailed derivation of the models.

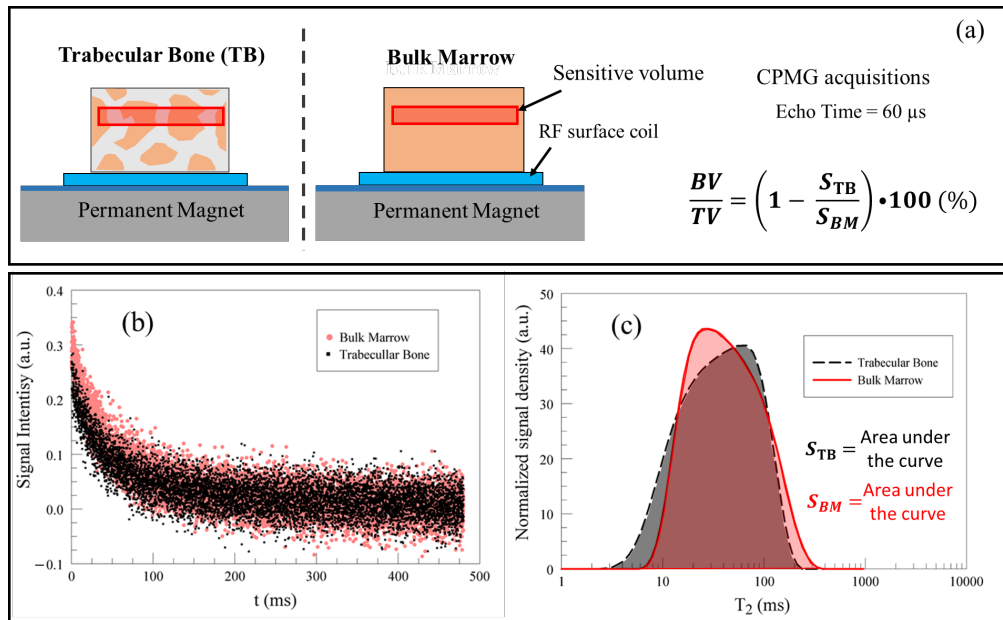


Figure 4. Evaluation of BV/TV ratio of trabecular bone in [47]. (a) Sketch of the experimental set-up; (b,c) pipeline used to evaluate the BV/TV ratio of trabecular bone; (b) signal intensity decays; (c) T_2 relaxation time distribution obtained by UpenWin software, implementing the Upen algorithm [63]. Since the experimental set was not optimized for SNR efficiency, the sub-millisecond decay component ascribed to the intra-trabecular bound, and pore water was not detected in the T_2 distribution so that it did not contribute to the signal.

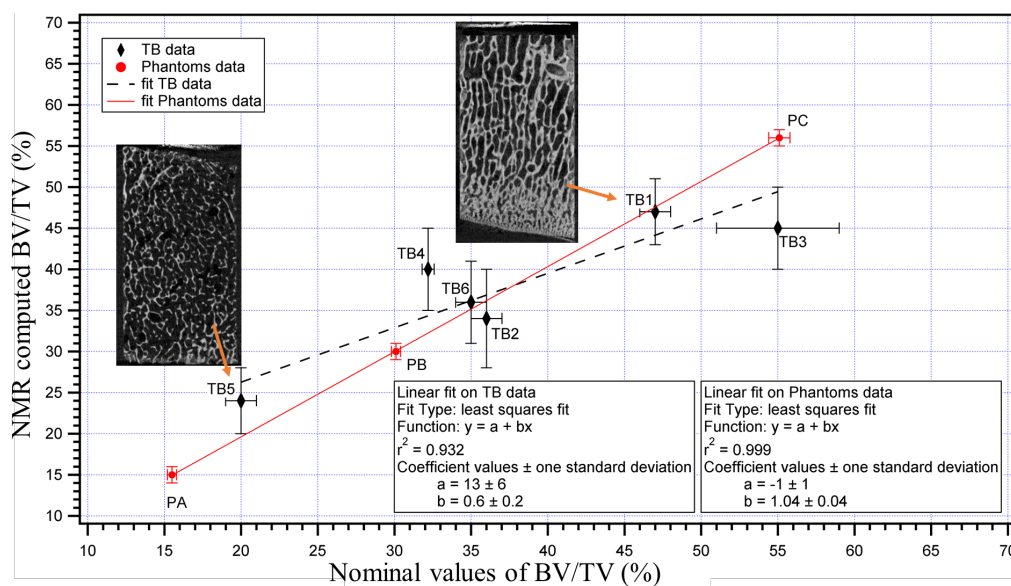


Figure 5. BV/TV values of TB animal samples and phantoms samples measured by single-sided scanner NMR-MOUSE PM10 (Magritek, Nz) vs. the nominal values. For the TB samples, the nominal values are the BV/TV values determined by the micro-CT analysis, whereas, for the phantoms, they have been obtained by the geometry of the samples. Examples of micro-CT images are reported for two TB samples. The figure was modified from reference [47]. Copyright (2017) Wiley, Copyright (Year) Wiley. Used with permission from reference [47].

The key idea was to exploit the information contained in the T_2 distribution of the trabecular bone sample computed from the acquired CPMG data to separate the intra-trabecular signal (due to water bound to collagen and pore water) and the signal coming from the inter-trabecular spaces (mainly due to bone marrow). This allowed one to compute the short T_2 intensity fraction, namely η , proportional to the volume occupied by fluids inside the trabeculae to the volume occupied by all fluids in the bone, including fluids within the spaces between the trabeculae. This parameter was found to strongly correlate with BV/TV and with the so-called bone surface density BS/TV, as shown in Figure 7a,b. Furthermore, the correlation between NMR and micro-CT estimated structural parameters showed a high level of agreement for BV/TV and a high correlation with a moderate agreement for BS/TV as summarized in Figure 7c,d, respectively. A further novelty of the work was demonstrating the possibility of quantifying with a single-sided NMR device the intra-trabecular porosity (see Figure 6c), a parameter not easy to measure by other methods. The study concluded that, for trabecular bones cored from the shoulder of healthy pigs, the average intra-trabecular porosity, ϕ_{tb} , was equal to $(30 \pm 5)\%$. The value of the intra-trabecular porosity was almost constant regardless of the BV/TV of the samples, which spanned the range (24–45)%.

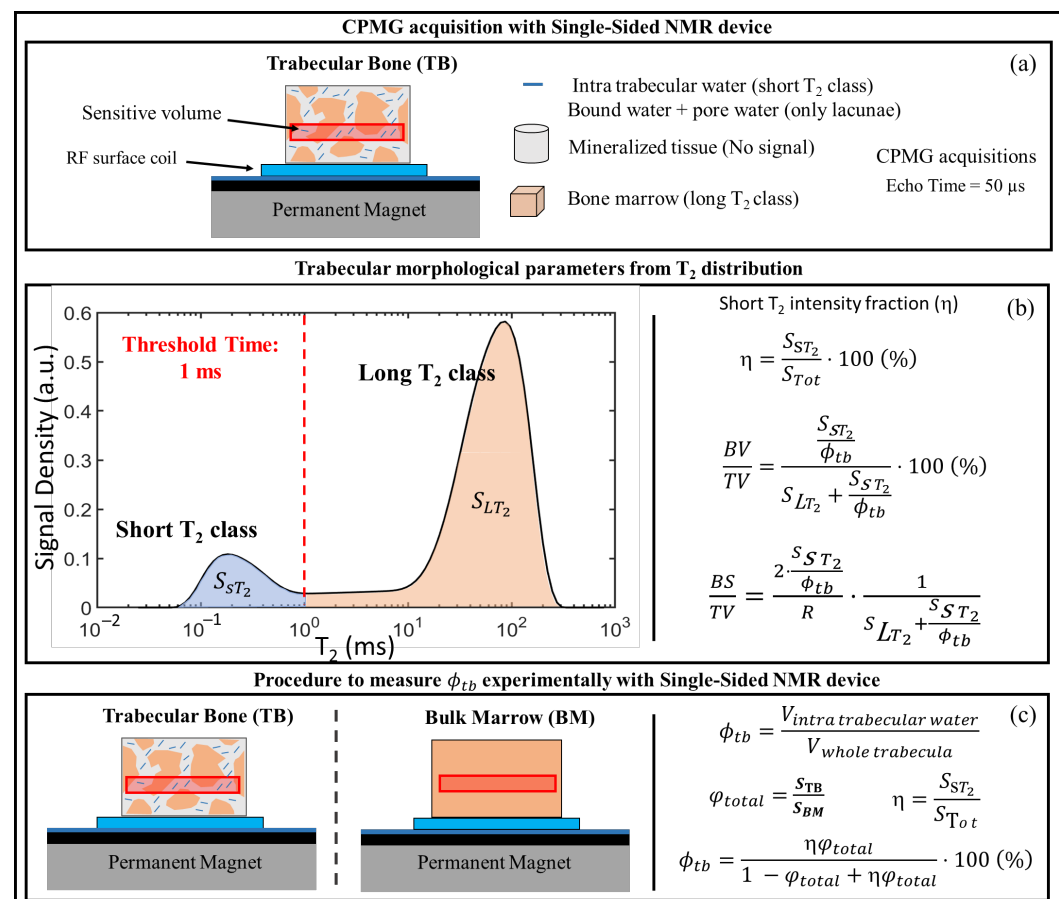


Figure 6. Sketch of the pipeline used in laboratory to evaluate the structural parameters of animal trabecular bone samples in [50]. (a) Experimental set-up; (b) separation on the T_2 distribution of the signal from ^1H inside the trabeculae from that coming from the marrow within the inter-trabecular spaces, through the definition of a threshold time, set at 1 ms. On the right, the theoretical relationships to estimate the two parameters BV/TV and BS/TS are summarized, starting from the computation of η , i.e., the ratio of the short T_2 signal to the total signal under the T_2 distribution. R is the average radius of the trabeculae, estimated from the average trabecular thickness, measured with micro-CT; (c) experimental procedure to measure the total porosity and the intra-trabecular porosity.

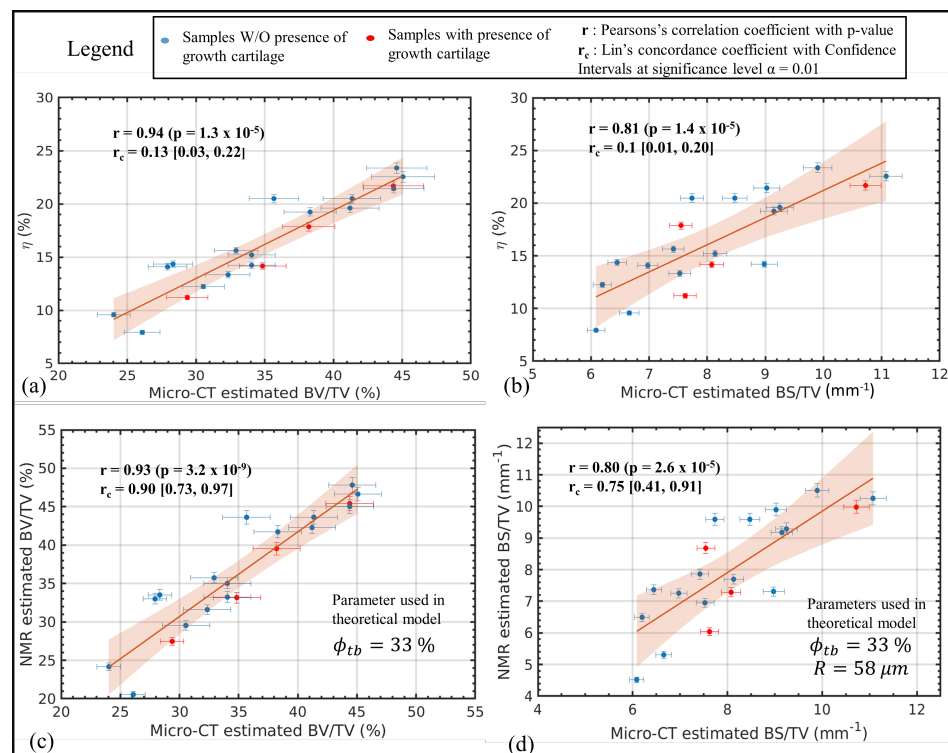


Figure 7. (top row) Plots of η , the short T_2 intensity fraction, evaluated using the quasi-continuous T_2 distributions, against the structural parameters evaluated by the micro-CT analyses. (a) the BV/TV; (b) the BS/TV (bottom row) Comparison between NMR and micro-CT estimated structural parameters; (c) BV/TV; (d) BS/TV. The average intra-trabecular porosity $\phi_{tb} = 33\%$, measured experimentally, was used in the theoretical models to estimate BV/TV and BS/TV with NMR. For the BS/TV, the trabeculae were modeled as cylinders and the average radius $R = 58 \mu\text{m}$, estimated from average trabecular thickness measured with micro-CT, was used. The figure was modified from reference [50]. Copyright (2020) Wiley. Used with permission from reference [50].

5. Discussion: Current Limitations and Future Perspectives

Obtaining information about the trabecular bone structure in addition to the BMD has been demonstrated to improve the fracture risk prediction associated with the osteoporosis disease. Methodologies able to gain this information in vivo, such as MRI-based methodologies, are not currently part of the clinical routine because of the high financial cost associated with MRI exams. NMR relaxometry has been demonstrated to be a well-suited methodology to study bone composition and structure. The ^1H nuclei present in the bone are found in different micro-environments, and their NMR signal contribution can be resolved in the T_2 quasi-continuous distributions. The use of portable single-sided NMR devices for biomedical applications is an emerging and appealing field because of their versatility and low purchasing and running costs. In this work, the state of the art of new methodologies that aimed to investigate trabecular bone structural properties exploiting a single-sided NMR device has been reviewed, highlighting the concepts behind the methods rooted in NMR relaxometry applied to the study of porous media.

The methodologies reviewed in this work showed that portable single-sided NMR devices could be efficiently utilized to retrieve structural information of trabecular bones in a laboratory study. A novelty of [50] was the demonstration of the possibility to quantify the intra-trabecular porosity, a parameter not easy to measure by other methods. The literature does not establish the extent to which diseases affecting bone tissue, such as osteoporosis, modify its structure at the intra-trabecular level. It is not clear whether the imbalanced and excessive bone remodeling that occurs in bone pathologies only affects the trabecular network, by removing some trabeculae, or whether it also affects the internal porosity of the trabeculae themselves. Hence, the technique can readily be used to investigate these

effects in laboratory studies exploiting a non-destructive methodology that uses low-cost portable single-sided NMR devices.

The long-term aim of these procedures is *in vivo* application for broad screening campaigns, but the methodology is still far from that goal. Some current limitations and challenges have to be addressed to move the technique forward. The main challenges related to an *in vivo* application of these techniques regard the correct positioning of the sensitive volume of the single-sided scanner within the chosen anatomical site. Commercially available single-sided NMR scanners have a maximum penetration depth of about 20 mm. With the envisage of application in humans, the limited achievable penetration depth would restrict the application of the technique to peripheral skeletal regions. In these anatomical sites, tissues other than trabecular bone, such as muscles or cartilage, may be present within the sensitive volume of the scanner affecting the correct estimation of structural parameters. A possible methodological solution is to explore the modification of the reviewed techniques to select only the signal coming from trabecular bone tissue by filtering out signal contributions from tissues surrounding the bone as investigated in [48]. In that work, the procedure proposed in [47] was modified using a suitable preparatory pulse sequence able to filter the signal in diffusion before the CPMG acquisition. This means to cancel out the signal from higher diffusion coefficient molecules before acquisition. The proposed modification correctly estimated the BV/TV of a trabecular bone sample even when muscle and cartilage tissues were present within the sensitive volume of the single-sided scanner. This was possible because water molecules in muscle and cartilage have diffusion coefficients about two orders of magnitude higher than those of fluids in bone marrow (mainly lipids). The concept of a diffusion filter, as proposed in [48], would not be straightforwardly applicable to the procedure developed in [50]. The diffusion preparation before the CPMG acquisition would also filter out the sub-millisecond T_2 components, components assigned to the water inside the trabeculae, which would eliminate the internal reference signal. New approaches that aim to integrate the concept of a diffusion filter without losing the information coming from the intra-trabecular water need to be further explored.

Another approach to face the challenges related to the positioning of the sensitive volume is to design an ad-hoc single-sided scanner for a specific bone district of interest. Thomas et al. [34,64] presented a novel single-sided NMR device with a maximum penetration depth of 50 mm, which was then successfully used to study brain hypoxia in an ovine model *in vivo*. These recent studies show that technological advances in the design of single-sided NMR scanners to reach the desired properties in terms of sensitive volume size, shape, and penetration depth are not just a matter of mere speculation. A single-sided NMR scanner with a penetration depth of a few cm allows for envisioning an application of the techniques reviewed here that is not only restricted to peripheral bones but could potentially be applied to other body regions of interest, such as the hip. Furthermore, augmented reality approaches can be explored to improve the proper positioning of the sensitive volume. Augmented and mixed reality frameworks have increased interest in the last years by combining 3D MRI or CT imaging with holographic vision devices for surgical planning [65–69]. However, these approaches require a 3D image of the anatomical site of interest, which is usually done through MRI or CT acquisitions. In the context of surgery planning, a 3D imaging modality is already necessary and part of the standard clinical routine. On the contrary, in the context of osteoporosis assessment, 3D imaging is not routinely applied. However, since recent works have shown the feasibility of rendering 3D bone shapes from 2D DXA scans [70,71], one can envision exploiting these methodologies as anatomical information to be combined with the augmented reality framework to improve the proper positioning of the sensitive volume of single-sided NMR devices within the anatomical site of interest. DXA scans are already routinely applied to assess bone health so that no additional financial costs and time would be required.

Lastly, the specific absorption rate (SAR) associated with the procedures reviewed in this work has not been studied. SAR measures the amount of radiofrequency power

absorbed per unit of mass of a tissue and needs to remain below specific levels to guarantee that a procedure does not cause excessive heating, resulting in burn injuries to patients. Measuring SAR is not trivial, but it scales with the square of the RF power. The methodology presented in [50] utilizes a CPMG with a train of 2000 refocusing pulses. Reducing the number of refocusing pulses will also reduce the RF power deposited in the tissue. The use of the log-spaced CPMG sequences [72,73], where the time delay between consecutive refocusing pulses is logarithmically spaced instead of being kept fixed, can be explored to reduce the number of pulses needed to sample the CPMG decay. It has been demonstrated that log-CPMG can accurately reproduce the T_2 distributions of rock samples where T_2 spanned the sub-millisecond–hundreds of milliseconds range [73]. Thus, log-CPMG may be a valuable tool to accommodate the SAR requirements that need to be met to apply the methodology in vivo.

In conclusion, this review gives grounds for confidence in the usefulness of single-sided NMR for studying bone porosity at different scale levels. The available techniques are considered mature for ex vivo preclinical investigation of the relationship between bone diseases, such as osteoporosis, and the structure of the bone, even at the intra-trabecular level. The methodology is still a long way from possible extension to an in vivo application. However, the challenges associated with this long-term aim have been discussed, and possible solutions to tackle each of these challenges have been proposed starting from readily available technology. This suggests that it is realistic to envisage future screening campaigns conducted on populations at risk of bone diseases, such as osteoporosis, using low-cost and portable single-sided NMR devices [74,75].

Author Contributions: Conceptualization: M.B., L.B. and P.F.; original draft preparation: M.B.; review and editing: M.B., P.F., C.T., V.B., F.B., F.K. and L.B. All authors contributed to the scientific discussion. All authors have read and agreed to the published version of the manuscript.

Funding: This research received no external funding.

Institutional Review Board Statement: Not applicable.

Informed Consent Statement: Not applicable.

Conflicts of Interest: M.B., P.F., C.T., V.B., F.B. and L.B. are coauthors of references [47,48,50]. The authors declare no other conflicts of interests.

Abbreviations

The following abbreviations are used in this manuscript:

BS/TV	Bone-surface to total-volume ratio
BV/TV	Bone-volume to total-volume ratio
CB	Cortical Bone
CPMG	Carr–Purcell–Meiboom–Gill
CT	Computed Tomography
HRqCT	High-Resolution quantitative Computed Tomography
MRI	Magnetic Resonance Imaging
NMR	Nuclear Magnetic Resonance
qMRI	quantitative Magnetic Resonance Imaging
qUS	quantitative Ultrasounds
TB	Trabecular Bone
Tb.Th	Trabecular Thickness

References

1. Avioli, L.V. Significance of osteoporosis: A growing international health care problem. *Calcif. Tissue Int.* **1991**, *49*, S5–S7. [[CrossRef](#)] [[PubMed](#)]
2. Krug, R.; Burghardt, A.J.; Majumdar, S.; Link, T.M. High-Resolution Imaging Techniques for the Assessment of Osteoporosis. *Radiol. Clin. N. Am.* **2010**, *48*, 601–621. [[CrossRef](#)] [[PubMed](#)]
3. Granke, M.; Makowski, A.J.; Uppuganti, S.; Does, M.D.; Nyman, J.S. Identifying Novel Clinical Surrogates to Assess Human Bone Fracture Toughness. *J. Bone Miner. Res.* **2015**, *30*, 1290–1300. [[CrossRef](#)] [[PubMed](#)]
4. Nazrun, A.; Tzar, M.; Mokhtar, S.; Mohamed, I. A systematic review of the outcomes of osteoporotic fracture patients after hospital discharge: Morbidity, subsequent fractures, and mortality. *Ther. Clin. Risk Manag.* **2014**, *10*, 937–948. [[PubMed](#)]
5. Choksi, P.; Jepsen, K.; Clines, G. The challenges of diagnosing osteoporosis and the limitations of currently available tools. *Clin. Diabetes Endocrinol.* **2018**, *4*, 937–948. [[CrossRef](#)]
6. Blake, G.M.; Fogelman, I. The role of DXA bone density scans in the diagnosis and treatment of osteoporosis. *Postgrad. Med. J.* **2007**, *83*, 509–517. [[CrossRef](#)]
7. Wainwright, S.A.; Marshall, L.M.; Ensrud, K.E.; Cauley, J.A.; Black, D.M.; Hillier, T.A.; Hochberg, M.C.; Vogt, M.T.; Orwoll, E.S. Hip Fracture in Women without Osteoporosis. *J. Clin. Endocrinol. Metab.* **2005**, *90*, 2787–2793. [[CrossRef](#)]
8. Kanis, J.; Johnell, O.; Oden, A.; Johansson, H.; McCloskey, E. FRAX™ and the assessment of fracture probability in men and women from the UK. *Osteoporos. Int.* **2008**, *19*, 385–397. [[CrossRef](#)]
9. Collins, G.S.; Mallett, S.; Altman, D.G. Predicting risk of osteoporotic and hip fracture in the United Kingdom: Prospective independent and external validation of QFractureScores. *BMJ* **2011**, *342*. Available online: <https://www.bmj.com/content/342/bmj.d3651.full.pdf> (accessed on 8 June 2021). [[CrossRef](#)]
10. Antich, P.P.; Anderson, J.A.; Ashman, R.B.; Dowdey, J.E.; Gonzales, J.; Murry, R.C.; Zenvekh, J.E.; Pak, C.Y. Measurement of mechanical properties of bone material in vitro by ultrasound reflection: Methodology and comparison with ultrasound transmission. *J. Bone Miner. Res.* **1991**, *6*, 417–426. [[CrossRef](#)]
11. Thomsen, K.; Jepsen, D.; Matzen, L.; Hermann, A.P.; Masud, T.; Ryg, J. Is calcaneal quantitative ultrasound useful as a prescreen stratification tool for osteoporosis? *Osteoporos. Int.* **2015**, *26*, 1459–1475. [[CrossRef](#)] [[PubMed](#)]
12. Hans, D.; Baim, S. Quantitative Ultrasound (QUS) in the Management of Osteoporosis and Assessment of Fracture Risk. *J. Clin. Densitom.* **2017**, *20*, 322–333. [[CrossRef](#)] [[PubMed](#)]
13. Ong, H.H.; Wright, A.C.; Wehrli, F.W. Deuterium nuclear magnetic resonance unambiguously quantifies pore and collagen-bound water in cortical bone. *J. Bone Miner. Res.* **2012**, *27*, 2573–2581. [[CrossRef](#)] [[PubMed](#)]
14. Fantazzini, P.; Brown, R.J.S.; Borgia, G.C. Bone tissue and porous media: Common features and differences studied by NMR relaxation. *Magn. Reson. Imaging* **2003**, *21*, 227–234. [[CrossRef](#)]
15. Fantazzini, P.; Bortolotti, V.; Brown, R.J.; Camaiti, M.; Garavaglia, C.; Viola, R.; Giavaresi, G. Two 1 H-nuclear magnetic resonance methods to measure internal porosity of bone trabeculae: By solid-liquid signal separation and by longitudinal relaxation. *J. Appl. Phys.* **2004**, *95*, 339–343. [[CrossRef](#)]
16. Sigmund, E.E.; Cho, H.; Song, Y.Q. High-resolution MRI of internal field diffusion-weighting in trabecular bone. *NMR Biomed.* **2009**, *22*, 436–448. [[CrossRef](#)]
17. Sprinkhuizen, S.M.; Ackerman, J.L.; Song, Y.Q. Influence of bone marrow composition on measurements of trabecular microstructure using decay due to diffusion in the internal field MRI: Simulations and clinical studies. *Magn. Reson. Med.* **2014**, *72*, 1499–1508. [[CrossRef](#)]
18. Mroue, K.H.; Nishiyama, Y.; Kumar Pandey, M.; Gong, B.; McNerny, E.; Kohn, D.H.; Morris, M.D.; Ramamoorthy, A. Proton-detected solid-state NMR spectroscopy of bone with ultrafast magic angle spinning. *Sci. Rep.* **2015**, *5*, 11991. [[CrossRef](#)]
19. Manhard, M.K.; Horch, R.A.; Harkins, K.D.; Gochberg, D.F.; Nyman, J.S.; Does, M.D. Validation of quantitative bound- and pore-water imaging in cortical bone. *Magn. Reson. Med.* **2014**, *71*, 2166–2171. [[CrossRef](#)]
20. Horch, R.A.; Gochberg, D.F.; Nyman, J.S.; Does, M.D. Clinically compatible MRI strategies for discriminating bound and pore water in cortical bone. *Magn. Reson. Med.* **2012**, *68*, 1774–1784. [[CrossRef](#)]
21. Du, J.; Bydder, G.M. Qualitative and quantitative ultrashort-TE MRI of cortical bone. *NMR Biomed.* **2013**, *26*, 489–506. [[CrossRef](#)]
22. Wehrli, F.W. Magnetic resonance of calcified tissues. *J. Magn. Reson.* **2013**, *229*, 35–48. [[CrossRef](#)] [[PubMed](#)]
23. Wehrli, F.W.; Song, H.K.; Saha, P.K.; Wright, A.C. Quantitative MRI for the assessment of bone structure and function. *NMR Biomed.* **2006**, *19*, 731–764. [[CrossRef](#)] [[PubMed](#)]
24. Ni, Q.; King, J.D.; Wang, X. The characterization of human compact bone structure changes by low-field nuclear magnetic resonance. *Meas. Sci. Technol.* **2004**, *15*, 58–66. [[CrossRef](#)]
25. Seifert, A.C.; Wehrli, S.L.; Wehrli, F.W. Bi-component T_2^* analysis of bound and pore bone water fractions fails at high field strengths. *NMR Biomed.* **2015**, *28*, 861–872. [[CrossRef](#)] [[PubMed](#)]
26. Fernández-Seara, M.A.; Song, H.K.; Wehrli, F.W. Trabecular Bone Volume Fraction Mapping by Low-Resolution MRI. *Magn. Reson. Med.* **2001**, *46*, 103–111. [[CrossRef](#)] [[PubMed](#)]
27. Iita, N.; Handa, S.; Tomiha, S.; Kose, K. Development of a compact MRI system for measuring the trabecular bone microstructure of the finger. *Magn. Reson. Med.* **2007**, *57*, 272–277. [[CrossRef](#)]
28. Blümich, B.; Blümler, P.; Eidmann, G.; Guthausen, A.; Haken, R.; Schmitz, U.; Saito, K.; Zimmer, G. The NMR-mouse: Construction, excitation, and applications. *Magn. Reson. Imaging* **1998**, *16*, 479–484. [[CrossRef](#)]

29. Manz, B.; Coy, A.; Dykstra, R.; Eccles, C.; Hunter, M.; Parkinson, B.; Callaghan, P. A mobile one-sided NMR sensor with a homogeneous magnetic field: The NMR-MOLE. *J. Magn. Reson.* **2006**, *183*, 25–31. [[CrossRef](#)]
30. Chang, W.H.; Chen, J.H.; Hwang, L.P. Single-sided mobile NMR with a Halbach magnet. *Magn. Reson. Imaging* **2006**, *24*, 1095–1102. [[CrossRef](#)]
31. Marble, A.E.; Mastikhin, I.V.; Colpitts, B.G.; Balcom, B.J. A compact permanent magnet array with a remote homogeneous field. *J. Magn. Reson.* **2007**, *186*, 100–104. [[CrossRef](#)]
32. Prado, P.J.; Blümich, B.; Schmitz, U. One-Dimensional Imaging with a Palm-Size Probe. *J. Magn. Reson.* **2000**, *144*, 200–206. [[CrossRef](#)]
33. García-Naranjo, J.C.; Mastikhin, I.V.; Colpitts, B.G.; Balcom, B.J. A unilateral magnet with an extended constant magnetic field gradient. *J. Magn. Reson.* **2010**, *207*, 337–344. [[CrossRef](#)]
34. Thomas, D.; Galvosas, P.; Teal, P.; Harrison, F.G.; Berry, M.; Tzeng, Y.; Obruchkov, S. Single sided magnet system for relaxometry and diffusion measurement. In Proceedings of the 28th ISMRM Annual Meeting, Honolulu, HI, USA, 18–24 April 2020.
35. Badea, E.; Şendrea, C.; Carşote, C.; Adams, A.; Blümich, B.; Iovu, H. Unilateral NMR and thermal microscopy studies of vegetable tanned leather exposed to dehydrothermal treatment and light irradiation. *Microchem. J.* **2016**, *129*, 158–165. [[CrossRef](#)]
36. Rehorn, C.; Blümich, B. Cultural Heritage Studies with Mobile NMR. *Angew. Chem. Int. Ed.* **2018**, *57*, 7304–7312. Available online: <https://onlinelibrary.wiley.com/doi/pdf/10.1002/anie.201713009> (accessed on 8 June 2021). [[CrossRef](#)] [[PubMed](#)]
37. Brizi, L.; Camaiti, M.; Bortolotti, V.; Fantazzini, P.; Blümich, B.; Haber-Pohlmeier, S. One and two-dimensional NMR to evaluate the performance of consolidants in porous media with a wide range of pore sizes: Applications to cultural heritage. *Microporous Mesoporous Mater.* **2018**, *269*, 186–190. [[CrossRef](#)]
38. Brizi, L.; Bortolotti, V.; Marmotti, G.; Camaiti, M. Identification of complex structures of paintings on canvas by NMR: Correlation between NMR profile and stratigraphy. *Magn. Reson. Chem.* **2020**, *58*, 889–901.
39. De Boever, E.; Foubert, A.; Oligschlaeger, D.; Claes, S.; Soete, J.; Bertier, P.; Özkul, M.; Virgone, A.; Swennen, R. Multiscale approach to (micro)porosity quantification in continental spring carbonate facies: Case study from the Cakmak quarry (Denizli, Turkey). *Geochem. Geophys. Geosyst.* **2016**, *17*, 2922–2939. Available online: <https://agupubs.onlinelibrary.wiley.com/doi/pdf/10.1002/2016GC006382> (accessed on 8 June 2021). [[CrossRef](#)]
40. Krüger, M.; Schwarz, A.; Blümich, B. Investigations of silicone breast implants with the NMR-MOUSE. *Magn. Reson. Imaging* **2007**, *25*, 215–218. [[CrossRef](#)] [[PubMed](#)]
41. Navon, G.; Eliav, U.; Demco, D.E.; Blümich, B. Study of order and dynamic processes in tendon by NMR and MRI. *J. Magn. Reson. Imaging* **2007**, *25*, 362–380. [[CrossRef](#)] [[PubMed](#)]
42. Rössler, E.; Mattea, C.; Stapf, S. Feasibility of high-resolution one-dimensional relaxation imaging at low magnetic field using a single-sided NMR scanner applied to articular cartilage. *J. Magn. Reson.* **2015**, *251*, 43–51. [[CrossRef](#)]
43. Rössler, E.; Mattea, C.; Saarakkala, S.; Lehenkari, P.; Finnilä, M.; Rieppo, L.; Karhula, S.; Nieminen, M.T.; Stapf, S. Correlations of low-field NMR and variable-field NMR parameters with osteoarthritis in human articular cartilage under load. *NMR Biomed.* **2017**, *30*, 1–14. [[CrossRef](#)]
44. Landeghem, M.V.; Danieli, E.; Perlo, J.; Blümich, B.; Casanova, F. Low-gradient single-sided NMR sensor for one-shot profiling of human skin. *J. Magn. Reson.* **2012**, *215*, 74–84. [[CrossRef](#)]
45. Ali, T.S.; Tourell, M.C.; Hugo, H.J.; Pyke, C.; Yang, S.; Lloyd, T.; Thompson, E.W.; Momot, K.I. Transverse relaxation-based assessment of mammographic density and breast tissue composition by single-sided portable NMR. *Magn. Reson. Med.* **2019**, *82*, 1199–1213. [[CrossRef](#)]
46. Rühli, F.J.; Böni, T.; Perlo, J.; Casanova, F.; Baias, M.; Egarter, E.; Blümich, B. Non-invasive spatial tissue discrimination in ancient mummies and bones in situ by portable nuclear magnetic resonance. *J. Cult. Herit.* **2007**, *8*, 257–263. [[CrossRef](#)]
47. Brizi, L.; Barbieri, M.; Baruffaldi, F.; Bortolotti, V.; Fersini, C.; Liu, H.; Nogueira d'Eurydice, M.; Obruchkov, S.; Zong, F.; Galvosas, P.; et al. Bone volume-to-total volume ratio measured in trabecular bone by single-sided NMR devices. *Magn. Reson. Med.* **2018**, *79*, 501–510. [[CrossRef](#)] [[PubMed](#)]
48. Barbieri, M.; Brizi, L.; Bortolotti, V.; Fantazzini, P.; Nogueira d'Eurydice, M.; Obruchkov, S.; Liu, H.; Galvosas, P. Single-sided NMR for the diagnosis of osteoporosis: Diffusion weighted pulse sequences for the estimation of trabecular bone volume fraction in the presence of muscle tissue. *Microporous Mesoporous Mater.* **2018**, *269*, 166–170. [[CrossRef](#)]
49. Brizi, L.; Barbieri, M.; Testa, C.; Fantazzini, P. ¹H nuclei compartmentalization, exchange and self-diffusion in cortical bone by one- and two-dimensions NMR in homogeneous and inhomogeneous fields. In Proceedings of the 27th ISMRM Annual Meeting, Montréal, QC, Canada, 11–16 May 2019.
50. Barbieri, M.; Fantazzini, P.; Bortolotti, V.; Baruffaldi, F.; Festa, A.; Manners, D.N.; Testa, C.; Brizi, L. Single-sided NMR to estimate morphological parameters of the trabecular bone structure. *Magn. Reson. Med.* **2021**, *85*, 3353–3369. Available online: <https://onlinelibrary.wiley.com/doi/pdf/10.1002/mrm.28648> (accessed on 8 June 2021). [[CrossRef](#)] [[PubMed](#)]
51. Haken, R.; Blümich, B. Anisotropy in Tendon Investigated in Vivo by a Portable NMR Scanner, the NMR-MOUSE. *J. Magn. Reson.* **2000**, *144*, 195–199. [[CrossRef](#)] [[PubMed](#)]
52. Bergman, E.; Sarda, Y.; Ritz, N.; Sabo, E.; Navon, G.; Bergman, R.; Nevo, U. In vivo assessment of aged human skin with a unilateral NMR scanner. *NMR Biomed.* **2015**, *28*, 656–666. [[CrossRef](#)] [[PubMed](#)]
53. Osterhoff, G.; Morgan, E.F.; Shefelbine, S.J.; Karim, L.; McNamara, L.M. Bone mechanical properties and changes with osteoporosis. *Injury* **2016**, *47*, S11–S20. [[CrossRef](#)]

54. Seeman, E. Bone quality: The material and structural basis of bone strength. *J. Bone Miner. Metab.* **2008**, *26*, 1–8. [CrossRef]
55. Zebaze, R.M.; Ghasem-Zadeh, A.; Bohte, A.; Iuliano-Burns, S.; Mirams, M.; Price, R.I.; Mackie, E.J.; Seeman, E. Intracortical remodelling and porosity in the distal radius and post-mortem femurs of women: A cross-sectional study. *Lancet* **2010**, *375*, 1729–1736. [CrossRef]
56. Appolonia, L.; Borgia, G.C.; Bortolotti, V.; Brown, R.J.S.; Fantazzini, P. Effects of hydrophobic treatments of stone on pore water studied by continuous distribution analysis of NMR relaxation times. *Magn Reson. Imaging* **2001**, *19*, 509. [CrossRef]
57. Song, Y.Q. Magnetic Resonance of Porous Media (MRPM): A perspective. *J. Magn. Reson.* **2013**, *229*, 12–24. [CrossRef] [PubMed]
58. Horch, R.A.; Gochberg, D.F.; Nyman, J.S.; Does, M.D. Non-invasive Predictors of Human Cortical Bone Mechanical Properties: T2Discriminated 1H NMR Compared with High Resolution X-ray. *PLoS ONE* **2011**, *6*, 1–5. [CrossRef] [PubMed]
59. Horch, R.A.; Nyman, J.S.; Gochberg, D.F.; Dortch, R.D.; Does, M.D. Characterization of 1H NMR signal in human cortical bone for magnetic resonance imaging. *Magn. Reson. Med.* **2010**, *64*, 680–687. [CrossRef]
60. Carr, H.; Purcell, E. Effects of diffusion on free precession in nuclear magnetic resonance experiments. *Phys. Rev.* **1954**, *94*, 630–638. [CrossRef]
61. Meiboom, S.; Gill, D. Modified spin-echo method for measuring nuclear relaxation times. *Rev. Sci. Instrum.* **1958**, *29*, 688–691. [CrossRef]
62. Cowin, S.C. Bone poroelasticity. *J. Biomech.* **1999**, *32*, 217–238. [CrossRef]
63. Borgia, G.; Brown, R.; Fantazzini, P. Uniform-Penalty Inversion of Multiexponential Decay Data. *J. Magn. Reson.* **1998**, *132*, 65–77. [CrossRef] [PubMed]
64. Thomas, D.; Harrison, F.G.; Teal, P.; Galvosas, P.; Berry, M.; Obruchkov, S.; Tzeng, Y. In vivo hypoxia monitoring using a novel single sided NMR device. In Proceedings of the 29th ISMRM Annual Meeting, Concord, CA, USA, 15–20 May 2021.
65. Perkins, S.L.; Lin, M.A.; Srinivasan, S.; Wheeler, A.J.; Hargreaves, B.A.; Daniel, B.L. A Mixed-Reality System for Breast Surgical Planning. In Proceedings of the 2017 IEEE International Symposium on Mixed and Augmented Reality (ISMAR-Adjunct), Nantes, France, 9–13 October 2017; pp. 269–274.
66. Ferrari, V.; Megali, G.; Troia, E.; Pietrabissa, A.; Mosca, F. A 3D Mixed-Reality System for Stereoscopic Visualization of Medical Dataset. *IEEE Trans. Biomed. Eng.* **2009**, *56*, 2627–2633. [CrossRef]
67. Gregory, T.M.; Gregory, J.; Sledge, J.; Allard, R.; Mir, O. Surgery guided by mixed reality: Presentation of a proof of concept. *Acta Orthop.* **2018**, *89*, 480–483. [CrossRef] [PubMed]
68. Neves, C.A.; Vaisbuch, Y.; Leuze, C.; McNab, J.A.; Daniel, B.; Blevins, N.H.; Hwang, P.H. Application of holographic augmented reality for external approaches to the frontal sinus. *Int. Forum Allergy Rhinol.* **2020**, *10*, 920–925. Available online: <https://onlinelibrary.wiley.com/doi/pdf/10.1002/alr.22546> (accessed on 8 June 2021). [CrossRef]
69. Sathyanarayana, S.; Leuze, C.; Hargreaves, B.; Daniel, B.; Wetzstein, G.; Etkin, A.; Bhati, M.T.; McNab, J.A. Comparison of head pose tracking methods for mixed-reality neuronavigation for transcranial magnetic stimulation. In Proceedings of the International Society for Optics and Photonics, SPIE: Medical Imaging 2020: Image-Guided Procedures, Robotic Interventions, and Modeling, Huston, TX, USA, 16 March 2020; Volume 11315, pp. 147–154.
70. Humbert, L.; Martelli, Y.; Fonollà, R.; Steghöfer, M.; Di Gregorio, S.; Malouf, J.; Romera, J.; Barquero, L.M.D.R. 3D-DXA: Assessing the Femoral Shape, the Trabecular Macrostructure and the Cortex in 3D from DXA images. *IEEE Trans. Med. Imaging* **2017**, *36*, 27–39. [CrossRef]
71. Väänänen, S.P.; Grassi, L.; Flivik, G.; Jurvelin, J.S.; Isaksson, H. Generation of 3D shape, density, cortical thickness and finite element mesh of proximal femur from a DXA image. *Med. Image Anal.* **2015**, *24*, 125–134. [CrossRef] [PubMed]
72. Ronczka, M.; Müller-Petke, M. Optimization of CPMG sequences to measure NMR transverse relaxation time T_2 in borehole applications. *Geosci. Instrum. Methods Data Syst.* **2012**, *1*, 197–208. [CrossRef]
73. Veselinovic, D.; Dick, M.; Green, D. Accurate Pore Size Measurement Via NMR On Unconventionals. In Proceedings of the Unconventional Resources Technology Conference, Denver, CO, USA, 22–24 July 2019; pp. 1878–1888. Available online: <https://library.seg.org/doi/pdf/10.15530/urtec-2019-394> (accessed on 8 June 2021).
74. Barbieri, M.; Watkins, L.; Desai, A.D.; Mazzoli, V.; Rubin, E.; Schmidt, A.; Gold, G.E.; Hargreaves, B.A.; Chaudhari, A.S.; Kogan, F. B_1 Field Inhomogeneity Correction for qDESS T_2 Mapping: Application to Rapid Bilateral Knee Imaging. In Proceedings of the 29th ISMRM Annual Meeting, Concord, CA, USA, 15–20 May 2021.
75. Barbieri, M.; Chaudhari, A.S.; Moran, C.J.; Gold, G.E.; Hargreaves, B.A.; Kogan, F. A Method for Measuring B_0 Field Inhomogeneity Using Quantitative DESS (qDESS). In Proceedings of the 29th ISMRM Annual Meeting, Concord, CA, USA, 15–20 May 2021.